The water entry of decelerating spheres

Jeffrey M. Aristoff,[1] Tadd T. Truscott,[2] Alexandra H. Techet,[3] and John W. M. Bush[4]
[1]*Department of Mechanical and Aerospace Engineering, Princeton University,
Princeton, New Jersey 08544, USA*
[2]*Naval Undersea Warfare Center, Newport, Rhode Island 02841, USA*
[3]*Department of Mechanical Engineering, Massachusetts Institute of Technology,
Cambridge, Massachusetts 02139, USA*
[4]*Department of Mathematics, Massachusetts Institute of Technology, Cambridge, Massachusetts 02139, USA*

We present the results of a combined experimental and theoretical investigation of the vertical impact of low-density spheres on a water surface. Particular attention is given to characterizing the sphere dynamics and the influence of its deceleration on the shape of the resulting air cavity. A theoretical model is developed which yields simple expressions for the pinch-off time and depth, as well as the volume of air entrained by the sphere. Theoretical predictions compare favorably with our experimental observations, and allow us to rationalize the form of water-entry cavities resulting from the impact of buoyant and nearly buoyant spheres. © *2010 American Institute of Physics.*
[doi:10.1063/1.3309454]

I. INTRODUCTION

When a solid object strikes a water surface, it may create an air cavity whose form influences the object's subsequent trajectory. Accurate models of this phenomenon are essential for the effective design of air-to-sea projectiles as may be used to target underwater mines, torpedoes, or enemy vessels.[1] A question of particular interest is how to design a supercavitating projectile that fits entirely within its own vapor cavity in order to achieve a drag-reduced state.[2] The water-entry problem is also relevant to applications in ship slamming,[3] stone skipping,[4] and the locomotion of water-walking creatures.[5] For a review of the water-entry literature, see Seddon and Moatamedi,[6] Aristoff and Bush,[7] and references therein. Theoretical modeling of water-entry cavities is typically simplified by examining high-density impacting bodies (such as steel spheres) that have negligible deceleration over the time scale of cavity collapse. In general, however, hydrodynamic forces cause impacting bodies to decelerate. Here, by examining low-density spheres that decelerate substantially following impact, we characterize both the deceleration rate and resulting change in the associated water-entry cavities.

Consider a solid sphere with density ρ_s and radius R_0 vertically impacting a horizontal water surface with speed U_0, as depicted in Fig. 1. Let g be the gravitational acceleration, ρ the liquid density, and η the dynamic viscosity. Provided that the Weber number $\mathcal{W} = \rho U_0^2 R_0 / \sigma \gg 1$, surface tension σ may be safely neglected and the impact characterized by the Froude number $\mathcal{F} = U_0^2 / (g R_0)$. Furthermore, provided that $\mathcal{F} \ll \rho / \rho_a$, where ρ_a is the air density, one may safely neglect aerodynamic pressure. In this limit, the impact creates an axisymmetric air cavity that expands radially before closing under the influence of hydrostatic pressure and eventually pinching off at depth. The impact is further characterized by the Reynolds number $\mathcal{R} = \rho U_0 R_0 / \eta \gg 1$, the

solid-liquid density ratio $\mathcal{D} = \rho_s / \rho$, the advancing contact angle θ_a, and the cavitation number $\mathcal{Q} = (p - p_v) / (1/2 \rho U_0^2)$, where p is the local water pressure and p_v is the water vapor pressure. In our study, $\mathcal{Q} \gg 1$, so the creation of cavitation bubbles in the liquid need not be considered.

The water-entry cavity formed by impacting bodies at high $\mathcal{W}$ has recently been investigated by Bergmann *et al.*,[8] Duclaux *et al.*,[9] and Truscott and Techet.[10] Bergmann *et al.*[8] considered the transient cavity created by the controlled impact of disks on a water surface at $1 < \mathcal{F} < 200$. Constant-speed descent was achieved by pulling the disks through the fluid with a motor. Duclaux *et al.*[9] considered the cavity created by freely falling spheres at $1 < \mathcal{F} < 80$ and introduced a theoretical model for the evolution of the cavity shape, a model extended by Aristoff and Bush[7] to account for aerodynamic pressure and surface tension, the latter being relevant for small impactors. Theoretical predictions for the pinch-off time and depth were found to be in good agreement with experiments using steel spheres whose deceleration could be neglected. A similar approach will be adopted in the present study, but here focus will be given to the influence of sphere deceleration on the cavity dynamics.

The importance of sphere deceleration (or acceleration) on the cavity evolution may be determined by considering the characteristic time scales associated with water entry. Let τ_p be the time scale of cavity collapse and τ_s the time scale over which the sphere decelerates (or accelerates) to a speed U^*. For buoyant spheres, $\rho_s / \rho \leq 1$, we take $U^* = 0$, and for $\rho_s / \rho > 1$, we take it to be the terminal speed of the sphere, $U^* \sim \sqrt{\Delta \rho g R_0 / \rho}$, where $\Delta \rho = \rho_s - \rho$. Let $m \sim \rho_s R_0^3$ be the sphere mass and $m_a \sim \rho R_0^3$ the added mass. Equating the product of the effective mass, $m + m_a$, and the characteristic sphere deceleration, $(U_0 - U^*) / \tau_s$, to the characteristic drag force, $\rho U_0^2 R_0^2$, yields
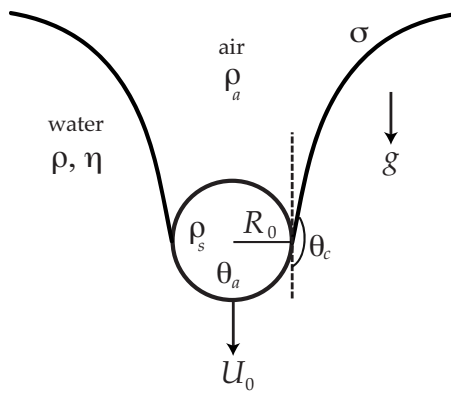
FIG. 1. Schematic of the impact parameters. The advancing contact angle is θ_a, and the cavity cone angle is θ_c.

FIG. 2. Schematic of the experimental apparatus.

$$\tau_s \frac{U_0}{R_0} \sim \begin{cases} \mathcal{D} + 1 & \text{for } \mathcal{D} \le 1 \\ (\mathcal{D} + 1)\left(1 - \sqrt{\dfrac{\mathcal{D}-1}{\mathcal{F}}}\right) & \text{for } \mathcal{D} > 1. \end{cases} \tag{1}$$

One may take for τ_p the pinch-off time predicted by Duclaux *et al.*[9] for the case of spheres sinking at constant speed: $\tau_p(U_0/R_0) \sim \mathcal{F}^{1/2}$. Provided that $\tau_s \gg \tau_p$, the sphere deceleration is negligible over the time scale of cavity collapse. Conversely, for $\tau_s \lesssim \tau_p$, the sphere dynamics necessarily influence the cavity evolution.

The characterization of sphere deceleration following impact has been considered by relatively few authors. The post-impact dynamics of a high $\mathcal{W}$ sphere with an attached air cavity has been investigated by May and Woodhull,[11] Lee *et al.*,[12] and Truscott and Techet.[10] May and Woodhull[11] estimated the drag coefficient, C_d, of steel spheres shot vertically into water and proposed the dependence $C_d = 0.0174 \ln(\mathcal{R}\mathcal{F}^{1/2})$ over the range of $500 < \mathcal{F} < 65\,000$ and $10^4 < \mathcal{R} < 10^6$. The applicability of this expression for use in our study is limited, however, as we shall be examining relatively low $\mathcal{F}$ impacts ($3 < \mathcal{F} < 100$). Lee *et al.*[12] considered the water entry of arbitrarily shaped projectiles and focused primarily on high $\mathcal{F}$ impacts ($\mathcal{F} > 150$). A theoretical model was developed by assuming that the kinetic energy lost by the projectile equals that fed into a horizontal fluid section and by approximating the combined effect of the projectile and the cavity on the fluid motion using distributed point sources along the vertical axis. At a given depth, their model predicts the cavity evolution only when the cavity diameter exceeds that of the projectile. Nonetheless, Lee *et al.* rationalized the observations of Gilbarg and Anderson[13] regarding the apparent independence of the dimensionless pinch-off time on the impact speed.

Truscott and Techet[10] investigated experimentally the water entry of both spinning and nonspinning spheres at $8 < \mathcal{F} < 340$. The authors provide further experimental evidence that the pinch-off time, $\tau_p \sim \sqrt{R_0/g}$ (or equivalently, $\tau_p(U_0/R_0) \sim \mathcal{F}^{1/2}$), is roughly constant even for spheres whose densities are comparable to that of water. However, they observed that the sphere depth at pinch-off decreases significantly with decreasing sphere density. A similar observation 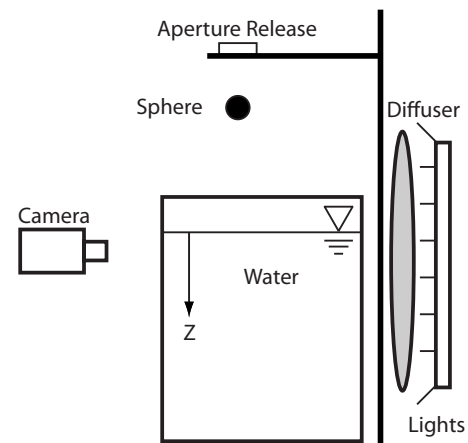was made by Gaudet[14] who presented numerical simulations of the water entry of circular disks at $1 < \mathcal{F} < 100$. He found that the pinch-off depth decreased with decreasing disk density and no longer scaled linearly with $\mathcal{F}^{1/2}$ as had been observed experimentally by Glasheen and McMahon[15] for disks whose speeds were roughly constant. In the present study, we extend the work of these authors by considering the water-entry cavity formed by decelerating spheres and developing a theoretical description thereof. Specifically, we develop a model for the sphere dynamics and deduce exact expressions for the cavity pinch-off time and pinch-off depth, as well as the volume of air entrained by the sphere.

II. EXPERIMENTAL STUDY

A schematic of our experimental apparatus is presented in Fig. 2. A sphere is held by a cameralike aperture at a height H above a water tank. The tank has dimensions of $30 \times 50 \times 60$ cm^3 and is illuminated by a bank of twenty 32-W fluorescent bulbs. A diffuser is used to provide uniform lighting, and care is taken to keep the water surface free of dust. The sphere is released from rest and falls toward the water, reaching it with approximate speed $U_0 \approx \sqrt{2gH}$. The impact sequence is recorded at 2000 frames/s using a high-speed camera. The resolution is set to 524×1280 pixels (px) with a field of view of 11.28×27.55 cm^2 yielding a 46.46 px/cm magnification. The trajectory of the sphere and its impact speed are determined with subpixel accuracy through a cross correlation and Gaussian peak-fitting method[10] yielding position estimates accurate to 0.025 px (0.0005 cm) and impact speeds accurate to $\pm 4\%$.

Six one-inch diameter spheres, each made from a different material, were used in the present study. Their densities are reported in Table I and range from 0.20 to 7.86 g cm^{-3}. In order to promote cavity formation, a hydrophobic spray coating, WX2100 by Cytonix LLC, Beltsville, MD, was used to prepare the spheres. Two coatings were applied, and the advancing contact angle was measured using the sessile drop method,[16] yielding values between 115° and 125°. Surface roughness measurements were made using a Tencor P-10 surface profilometer, and the root mean square (rms) displacements of the roughness profiles were computed. The

TABLE I. Densities of the spheres used in our study. Each sphere has a diameter of 2.54 ± 0.005 cm, an advancing contact angle of $120 \pm 5°$, and a characteristic roughness of 1 μm.

Material	Density ratio ($\mathcal{D} = \rho_s / \rho$)
Steel ($\diamond$)	7.86
Teflon ($\bigcirc$)	2.30
Delrin ($\bigtriangledown$)	1.41
Nylon ($\triangle$)	1.14
Polypropylene ($\square$)	0.86
Hollow polypropylene	0.20

hydrophobic coatings applied to each sphere gave rise to a roughness rms of the order of 1 μm. The coatings did not appreciably affect the sphere diameter or density.

Each sphere was released from 11 different heights. Below the minimum release height, 2 cm, air cavities were not reliably formed upon water entry.[17] Above the maximum release height, 65 cm, pinch-off at depth ("deep seal") did not

occur prior to the splash curtain closing the cavity from above ("surface seal"). In our experiments, the Froude number thus ranges from $\mathcal{F} = 3$ to 100 and Reynolds number from $\mathcal{R} = 10^3$ to 10^5. Weber numbers ranged from $\mathcal{W} = 70$ to 2300, so surface tension can be safely neglected.

The impact of a sphere that creates a subsurface air cavity has several distinct features. Figure 3 shows a time series of four impacting spheres that differ in density but have the same radius and impact speed ($\mathcal{F} = 38$, $\mathcal{W} = 854$). An axisymmetric cavity is evident below the surface and a splash curtain above. The evolution of the splash curtain is described by Aristoff and Bush.[7] The cavity adjoins the sphere near its equator, and its radial extent is of the order of the sphere radius. As the sphere descends, it transfers momentum to the fluid by forcing it radially outward. This inertial expansion of the fluid is resisted by hydrostatic pressure, which eventually reverses the direction of the radial flow, thereby initiating cavity collapse. The collapse accelerates until the moment of pinch-off, at which the cavity is divided into two separate cavities. The upper cavity continues col-
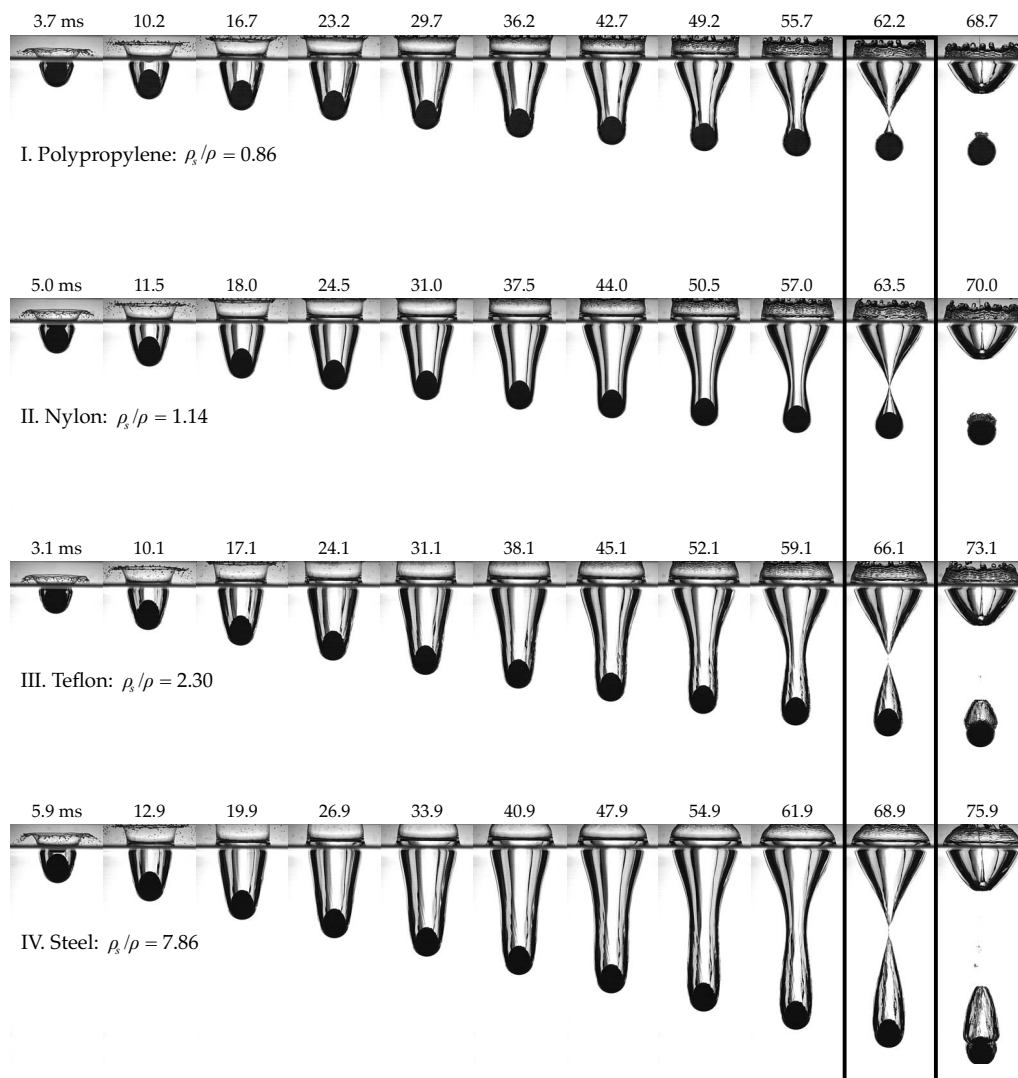

FIG. 3. Image sequences showing the water-entry cavity formed by four spheres with different densities. The radius (1.27 cm) and impact speed (217 cm s^{-1}) were held constant ($\mathcal{F} = 38$, $\mathcal{W} = 854$), while the density ratio $\mathcal{D} = \rho_s / \rho$ was increased through (I) 0.86, (II) 1.14, (III) 2.30, and (IV) 7.86. Times since the sphere center passed the free surface ($t = 0$) are shown.
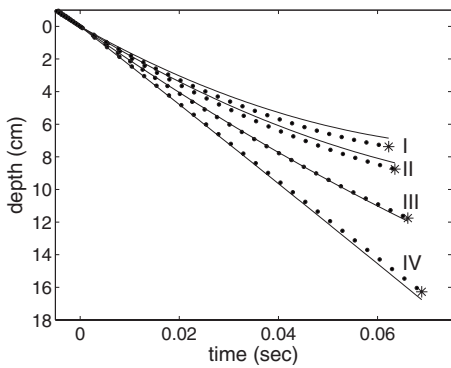
FIG. 4. Measured mean sphere depth vs time for the four impact sequences shown in Fig. 3. Every fifth data point is shown. The solid curves denote the theoretically predicted trajectories and are given by Eq. (8) for $C_m=0.25$ and $C_d=0.07$. The pinch-off event is denoted by *.

lapsing in such a way that a vigorous vertical jet is formed that may ascend well above the initial drop height of the sphere.[18] The lower cavity remains attached to the sphere and may undergo oscillations.[19] A relatively weak downward jet may also be observed to penetrate this lower cavity from above.

The most obvious differences between the four impact sequences are the trajectories of the spheres, shown in Fig. 4, and the cavity shapes near pinch-off, as are highlighted in Fig. 3. As the sphere density decreases, several trends are readily apparent. First, the depth of pinch-off decreases. Second, the depth of the sphere at pinch-off decreases. Third, the pinch-off depth approaches the sphere depth at pinch-off. Finally, the pinch-off time decreases. These trends are further explored in Fig. 5, where we report these pinch-off characteristics for each of the water-entry cavities. Let us first consider the pinch-off time, pinch-off depth, and sphere depth at pinch-off. While we observe roughly linear relationships between these dimensionless quantities and $\mathcal{F}^{1/2}$ for the heaviest (steel) spheres, these relationships become nonlinear as the sphere density decreases. The dependence on sphere density of the pinch-off characteristics is most pronounced for the sphere depth at pinch-off and least for the pinch-off time. The observed pinch-off depth relative to the sphere depth is shown in Fig. 5(d) and also exhibits a dependence on density.
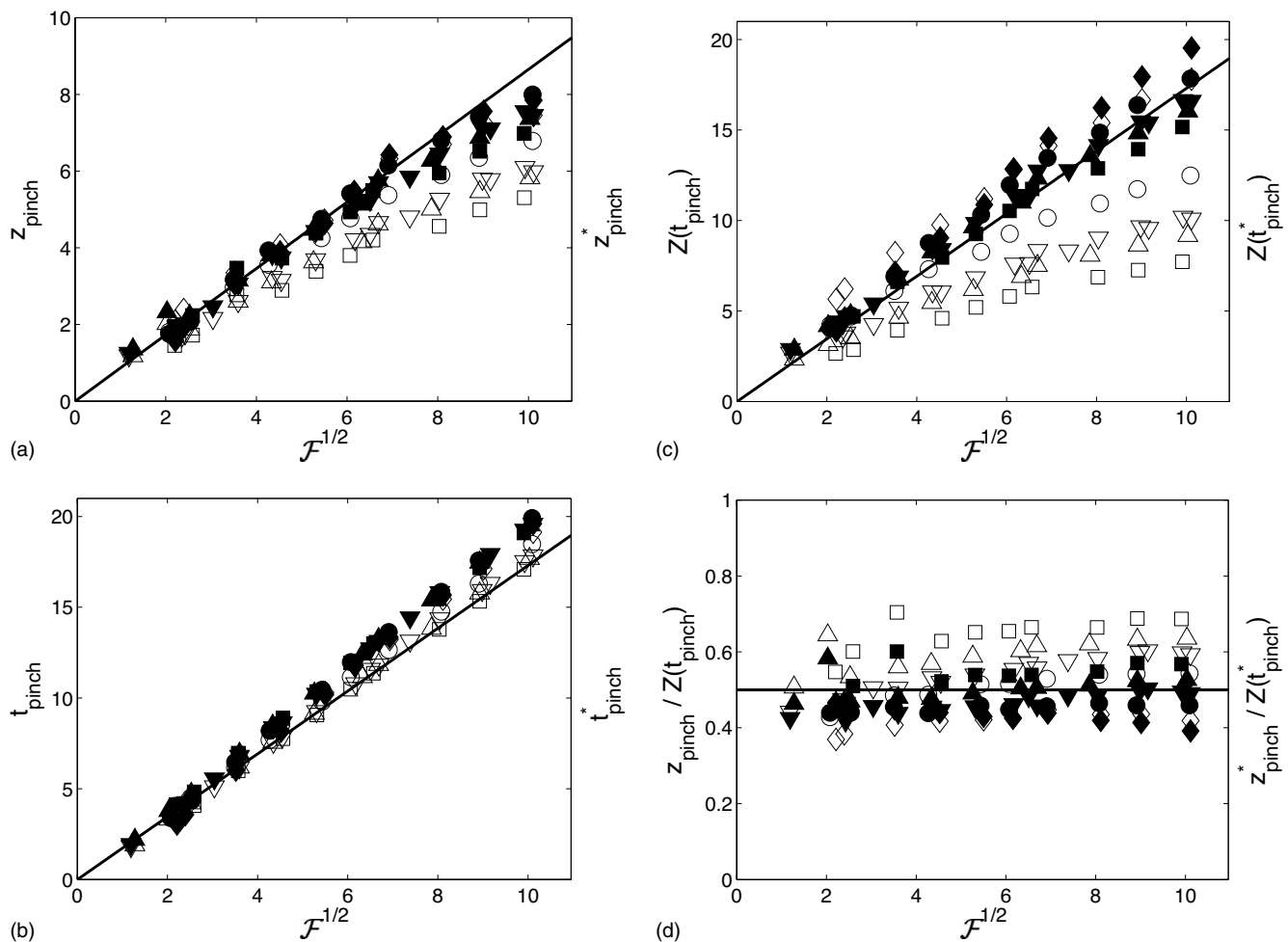

FIG. 5. Characteristics of the water-entry cavity formed by decelerating spheres. The hollow symbols denote the dependence on $\mathcal{F}^{1/2}$ of the (a) pinch-off depth z_{pinch}, (b) pinch-off time t_{pinch}, (c) sphere depth at pinch-off $Z(t_{pinch})$, and (d) ratio between the pinch-off depth and the sphere depth at pinch-off $z_{pinch}/Z(t_{pinch})$. The black symbols denote these same quantities when corrected for the average sphere deceleration Λ, specifically at (a) $z^*_{pinch}=z_{pinch}+\Lambda(\sqrt{\alpha}\mathcal{F}+\sqrt{2}\alpha^{1/4}\mathcal{F}^{1/2})$, (b) $t^*_{pinch}=t_{pinch}+\Lambda(\sqrt{\alpha}\mathcal{F}+2\sqrt{2}\alpha^{1/4}\mathcal{F}^{1/2})$, (c) $Z(t^*_{pinch})=Z(t_{pinch})+\Lambda(5\sqrt{\alpha}\mathcal{F}+2\sqrt{2}\alpha^{1/4}\mathcal{F}^{1/2})$, and (d) $z^*_{pinch}/Z(t^*_{pinch})=z_{pinch}/Z(t_{pinch})+\Lambda(\frac{3\sqrt{2}}{8}\alpha^{1/4}\mathcal{F}^{1/2})$. The solid lines denote the theoretical predictions and are given respectively by Eqs. (18)–(21) for $\alpha=0.14$. Symbols indicate different density ratios $\mathcal{D}=\rho_s/\rho$: $\square$, $\mathcal{D}=0.86$; $\triangle$, $\mathcal{D}=1.14$; $\triangledown$, $\mathcal{D}=1.41$; $\bigcirc$, $\mathcal{D}=2.30$; and $\diamond$, $\mathcal{D}=7.86$. The error in measurement is of the order of the symbol size.
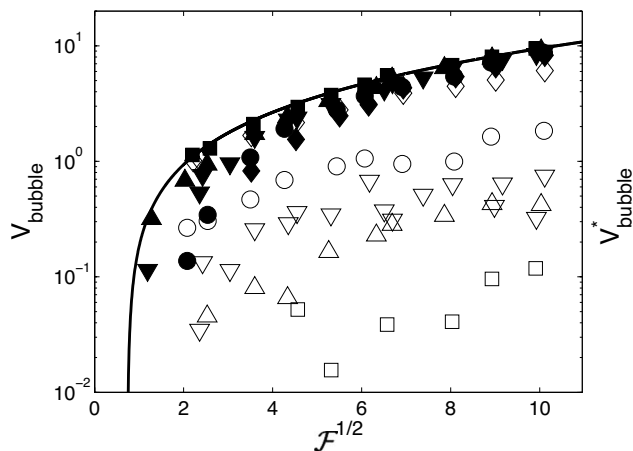
FIG. 6. Dependence on $\mathcal{F}^{1/2}$ of the volume of air entrained by the sphere, $V_{bubble} = V'_{bubble}/(\frac{4}{3}\pi R_0^3)$. The hollow symbols denote the measured bubble volume. The black symbols denote this same quantity when corrected for the average sphere deceleration Λ, specifically, $V^*_{bubble} = V_{bubble} + \Lambda(\frac{3\sqrt{2}}{4}\alpha^{1/4}\mathcal{F}^{1/2} + \frac{11\sqrt{2}}{10}\alpha^{5/4}\mathcal{F}^{3/2} + \frac{1}{2}\alpha\mathcal{F} + 3\sqrt{\alpha}\mathcal{F})$. The solid curve denotes the theoretically predicted bubble volume and is given by Eq. (23) for $\alpha = 0.14$. Symbols indicate different density ratios $\mathcal{D} = \rho_s/\rho$: $\square$, $\mathcal{D} = 0.86$; $\triangle$, $\mathcal{D} = 1.14$; $\triangledown$, $\mathcal{D} = 1.41$; $\bigcirc$, $\mathcal{D} = 2.30$; and $\diamond$, $\mathcal{D} = 7.86$. The error in the measurement of volume is ± 0.1 cm^3, that is, roughly 1% of the sphere volume.

Finally, in Fig. 6 we report the volume of air entrained by the sphere, specifically, the volume of the lower cavity at the time of pinch-off. We note that no air entrainment was observed for impacts for which $\mathcal{F} < 4$.

We note that in Figs. 5 and 6, we have excluded impacts for which pinch-off was obstructed by the sphere, corresponding to the water entry of the lightest sphere, an example of which is shown in Fig. 7. The sphere ascends in the fluid column before pinch-off, thereby obstructing collapse of the cavity.

III. THEORETICAL MODEL

We first consider the deceleration of the sphere and then the evolution of its water-entry cavity. Following impact, the sphere sinks under the combined influence of gravity and its own inertia and is resisted by buoyancy and hydrodynamic forces, respectively, F'_b and F'_d. A vertical force balance on the sphere may be expressed as

$$(m + m_a)\ddot{Z}' = mg - F'_b - F'_d, \tag{2}$$

where $Z'(t')$ is the depth of the center of the sphere, $m = \frac{4}{3}\rho_s\pi R_0^3$ is the sphere mass, $\ddot{Z}'$ is its acceleration, and primes denote dimensional quantities. The force required to accelerate the surrounding fluid is expressed in terms of an added mass, $m_a = C_m\rho V$, where C_m is the added mass coefficient, and V is the sphere volume. While we expect C_m to increase from zero at impact,[20] for the sake of simplicity we assume a constant value, corresponding to its mean over depths $0 \leq Z \leq Z^*$, where Z^* is the maximum depth reached by the sphere prior to its cavity pinching off. A simple model for the sphere dynamics is obtained by assuming that the cavity adjoins the sphere at its equator so that $F'_b = \pi R_0^2 \rho g Z' + \frac{2}{3}\pi R_0^3 \rho g$ is the upward buoyant force due to hydrostatic pressure and $F'_d = \frac{1}{2}\rho\dot{Z}'|\dot{Z}'|C_d\pi R_0^2$ is the resisting force due to form drag. The drag coefficient, C_d, is typically taken to be constant with respect to the impact parameters and penetration depth in studies of subsonic water entry,[12] and we shall do likewise. Substituting the dimensionless variables $Z = Z'/R_0$ and $t = t'U_0/R_0$ into Eq. (2) yields

$$\ddot{Z} = a - bZ - c\dot{Z}|\dot{Z}|, \tag{3}$$

where

$$a = \frac{\mathcal{D} - 1/2}{\mathcal{F}(\mathcal{D} + C_m)}, \quad b = \frac{3}{4\mathcal{F}(\mathcal{D} + C_m)}, \quad \text{and} \quad c = \frac{3C_d}{8(\mathcal{D} + C_m)}. \tag{4}$$

Integrating Eq. (3) once in Z gives an expression for the sphere speed,

$$U(Z) = \pm\sqrt{\left[\tilde{U}^2 - \frac{b}{2c^2} - \text{sign}(U)\left(\frac{a}{c}\right)\right]e^{-2c\,\text{sign}(U)Z} + \frac{b}{2c^2} + \text{sign}(U)\left(\frac{a - bZ}{c}\right)}, \tag{5}$$

where we have used the initial condition $U(Z=0) = \tilde{U}$.

We characterize the sphere dynamics with its mean deceleration, Λ, over depths $0 \leq Z \leq Z^*$. The value for Λ is found by using Eqs. (3) and (5),
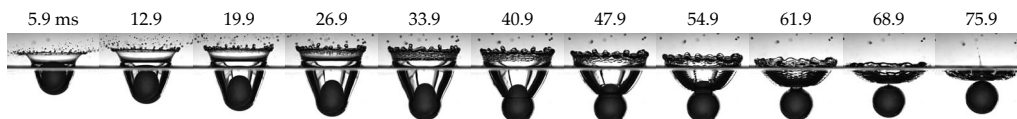

FIG. 7. Image sequence of the water-entry cavity formed by a hollow polypropylene sphere with density $\rho_s = 0.20$ g cm^{-3}, radius $R_0 = 1.27$ cm, and impact speed $U_0 = 240$ cm s^{-1}. $\mathcal{F} = 46$ and $\mathcal{W} = 1120$. This is an example of obstructed collapse in which the sphere reverses direction prior to pinch-off.

$$\Lambda = -\frac{1}{Z^*}\int_0^{Z^*}(a - bZ - cU^2)dZ$$

$$= \frac{(2c^2\tilde{U}^2 - 2ac - b)(1 - e^{-2cZ^*}) + 2bcZ^*}{4c^2Z^*}. \tag{6}$$

The sphere trajectory is then simply described by the quadratic function

$$Z(t) = -\frac{\Lambda}{2}t^2 + \tilde{U}t. \tag{7}$$

For spheres whose speed does not change sign prior to pinch-off, including negatively buoyant spheres, $Z^* = Z(t_{\text{pinch}})$ is the sphere depth at pinch-off. Conversely, for sufficiently buoyant spheres, Z^* may be found by solving $U(Z^*) = 0$ using Eq. (5).

In our subsequent analysis, we take the dimensional sphere speed when it is half-submerged, $\tilde{U}'$, to be $U_0\sqrt{1 - 2\Lambda}$ so that Eq. (7) becomes

$$Z(t) = -\frac{\Lambda}{2}t^2 + \sqrt{1 - 2\Lambda}\,t. \tag{8}$$

By doing so, we enforce the impact condition $U(Z = -1) = 1$ and thereby approximate the sphere deceleration as Λ over depths $-1 \leq Z < 0$ and in addition to over depths $0 \leq Z \leq Z^*$. An explicit expression for Λ may now be obtained by substituting

$$\tilde{U} = \sqrt{1 - 2\Lambda} \tag{9}$$

into Eq. (6) and solving for Λ,

$$\Lambda = \frac{(2bcZ^* - 2ac - b + 2c^2)e^{2cZ^*} + 2ac + b - 2c^2}{4c^2[(Z^* + 1)e^{2cZ^*} - 1]}. \tag{10}$$

Differentiating Eq. (8) gives the sphere speed,

$$U(Z) = \pm\sqrt{1 - 2\Lambda - 2\Lambda Z}. \tag{11}$$

The solid curves in Fig. 4 denote the sphere trajectories predicted by Eq. (8). We note that in our experiments, $|U_0 - \tilde{U}'|/U_0$ can be as much as 0.10, and thus it would be inadequate to take $\tilde{U}'$ as the impact speed.

In Fig. 8, we compare the measured average deceleration from each experiment to that predicted by Eq. (10), where we take Z^* to be the measured sphere depth at pinch-off. In each reference to Eq. (10), we choose $C_m = 0.25$, half the value appropriate for a sphere moving in an unbounded fluid,[21] and choose $C_d = 0.07$, the drag coefficient that minimizes the sum of squares of the error between the predicted and measured average decelerations. The low coefficient of drag suggests that the sphere and cavity perform similar to a streamlined body. Note that we do not include data for experiments with $\mathcal{D} = 0.20$ in which the contact line advances beyond the equator, as our model does not account for such motion. The agreement between experimental observations and theoretical predictions suggests that Eq. (8) provides an adequate description of the sphere dynamics. A similar agreement is obtained by instead choosing $C_m = 0.5$ and $C_d = 0.11$, indicating that the model is not highly sensitive to our
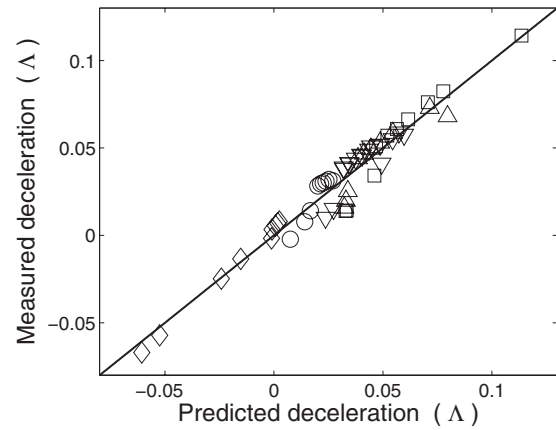

FIG. 8. The dimensionless average deceleration, Λ, of a sphere upon water entry. The theoretically predicted deceleration is given by Eq. (10) for $C_m = 0.25$ and $C_d = 0.07$. Symbol types correspond to the density ratios $\mathcal{D} = \rho_s/\rho$: $\square$, $\mathcal{D} = 0.86$; $\triangle$, $\mathcal{D} = 1.14$; $\triangledown$, $\mathcal{D} = 1.41$; $\bigcirc$, $\mathcal{D} = 2.30$; and $\diamond$, $\mathcal{D} = 7.86$. The error in the measurement of average deceleration is $\pm 0.1\%$.

choice of C_m and C_d. We note that the theoretically predicted sphere depth at pinch-off [to be defined subsequently by Eq. (17)] could also be used together with Eq. (10) to determine Λ.

The evolution of an axisymmetric water-entry cavity is amenable to analytical treatment if one assumes a purely radial motion, $ru = R\dot{R}$, prescribed by that of the cavity walls having radial speed $\dot{R}(t, z)$, where r is the radial coordinate and u is the radial component of the fluid velocity. Using the corresponding velocity potential, together with the Bernoulli equation, Duclaux *et al.*[9] obtained an approximate expression for the evolution of the cavity wall $R(t, z)$ at depth z,

$$\frac{d^2(R^2)}{dt^2} = -\frac{2z}{\mathcal{F}}, \tag{12}$$

where lengths are nondimensionalized by R_0 and time by R_0/U_0. In so doing, Duclaux *et al.* made the following assumptions: (1) the radial extent of the fluid motion is of the order of the sphere radius, (2) the contact line is pinned at the equator of the sphere, and (3) the initial radial speed of the cavity wall is proportional to the sphere speed. Thus, the boundary conditions for Eq. (12) become $R(t = 0) = 1$ and $\dot{R}(t = 0) = \sqrt{\alpha}U(z)$, where $U(z)$ is the sphere speed at depth z. The parameter α is related to the cavity cone angle, θ_c (see Fig. 1), by geometry, $\alpha = \cot^2[\theta_c - (\pi/2)]$. We take α to be constant, as is consistent with our experimental observation that $\theta_c \approx 160°$, and with a previous observation that α is relatively independent of $\mathcal{F}$.[8] Integrating Eq. (12) yields the evolution equation

$$R(t, z) = \sqrt{-\frac{z}{\mathcal{F}}t^2 + 2\sqrt{\alpha}Ut + 1}. \tag{13}$$

The assumed form of the velocity potential neglects the three-dimensionality of the flow that one expects to be non-negligible in the near-surface region. Thus, the ability of Eq. (13) to predict the cavity shapes for $z < 1$ is limited. However, Eq. (13) may safely be used to predict the pinch-off depth (and time) for sufficiently deep pinch-off.

The pinch-off time is the minimum time over depths $0 < z < \infty$ of the cavity collapse,

$$t_{\text{pinch}} = \min_{0 < z < \infty} [t(z) + t_c(z)], \quad (14)$$

where $t(z)$ is the time taken for the sphere to arrive at depth z and $t_c(z)$ is the collapse time for a particular depth. Using Eqs. (13) and (14), Duclaux et al.[9] obtained expressions for the pinch-off time and depth in the limit where the sphere deceleration can be neglected, $\Lambda \to 0$, corresponding to the water entry of dense spheres, $\mathcal{D} \gg 1$.

We here examine the influence of the sphere deceleration on its water-entry cavity. First, the inception time of the cavity at a given depth is delayed; second, the speed at which fluid is flung radially outward is reduced. Thus, in the expression for the pinch-off time, Eq. (14), $t(z)$ increases while $t_c(z)$ decreases. Using our approximation for the sphere speed, Eq. (11), we solve Eq. (13) for t when $R = 0$ to obtain an expression for collapse time at a given depth,

$$t_c(z) = \frac{2\mathcal{F}\sqrt{\alpha}\sqrt{1 - 2\Lambda - 2\Lambda z}}{z}. \quad (15)$$

In writing Eq. (15), we have taken the limit relevant to our experiments, $\alpha U^2 \mathcal{F}/z \gg 1$, corresponding to the regime in which the cavity expands before collapsing.

Provided that the radial collapse of the cavity is unobstructed by the sphere, we may substitute Eq. (15) into Eq. (14) along with $t(z)$, obtained from Eq. (8), to write

$$t_{\text{pinch}} = \min_{0 < z < \infty} \left(\frac{\sqrt{1 - 2\Lambda} - \sqrt{1 - 2\Lambda - 2\Lambda z}}{\Lambda} \right.$$
$$\left. + \frac{2\mathcal{F}\sqrt{\alpha}\sqrt{1 - 2\Lambda - 2\Lambda z}}{z} \right). \quad (16)$$

By solving Eq. (16), we find the pinch-off depth

$$z_{\text{pinch}} = \alpha^{1/4}\mathcal{F}^{1/2}\sqrt{\sqrt{\alpha}\mathcal{F}\Lambda^2 - 4\Lambda + 2} - \sqrt{\alpha}\mathcal{F}\Lambda. \quad (17)$$

A first-order Taylor series expansion of Eq. (17) about $\Lambda = 0$ yields

$$z_{\text{pinch}} = \sqrt{2}\alpha^{1/4}\mathcal{F}^{1/2} - \Lambda(\sqrt{\alpha}\mathcal{F} + \sqrt{2}\alpha^{1/4}\mathcal{F}^{1/2}). \quad (18)$$

Similarly, the pinch-off time, $t(z_{\text{pinch}}) + t_c(z_{\text{pinch}})$, is given by

$$t_{\text{pinch}} = 2\sqrt{2}\alpha^{1/4}\mathcal{F}^{1/2} - \Lambda(\sqrt{\alpha}\mathcal{F} + 2\sqrt{2}\alpha^{1/4}\mathcal{F}^{1/2}) \quad (19)$$

and the sphere depth at pinch-off by

$$Z(t_{\text{pinch}}) = 2\sqrt{2}\alpha^{1/4}\mathcal{F}^{1/2} - \Lambda(5\sqrt{\alpha}\mathcal{F} + 2\sqrt{2}\alpha^{1/4}\mathcal{F}^{1/2}). \quad (20)$$

The pinch-off depth relative to the sphere depth at pinch-off may then be expressed as

$$\frac{z_{\text{pinch}}}{Z(t_{\text{pinch}})} = \frac{1}{2} + \frac{3\sqrt{2}}{8}\alpha^{1/4}\mathcal{F}^{1/2}\Lambda. \quad (21)$$

We note that the theoretical predictions given by Eqs. (15)–(21) reduce to those of Duclaux et al.[9] for $\Lambda = 0$, corresponding to the limit of constant sphere speed.

In Fig. 5 we present a quantitative comparison between experiment and theory for cases of unobstructed cavity collapse. The solid lines denote the theoretical predictions given by Eqs. (18)–(21). The black symbols denote the experimentally observed pinch-off characteristics when corrected for the sphere deceleration ($\Lambda \neq 0$), the white symbols when deceleration is neglected ($\Lambda = 0$). By considering the sphere decelerations, the agreement between experiment and theory is significantly improved. We note that the exception is the pinch-off time [Fig. 5(b)], for which the agreement is comparable, but still within our experimental uncertainty. In addition, we observe that a linear relationship between the pinch-off depth and $\mathcal{F}^{1/2}$ is valid only for the impact of high-density spheres whose decelerations can be neglected. The same can be said for the $\mathcal{F}$-dependence of the sphere depth at pinch-off. In Fig. 5(a), the discrepancy at high $\mathcal{F}$ is likely due to the neglect of aerodynamic pressure in our derivation of Eq. (12), which would tend to decrease the pinch-off depth.

Our theoretical model captures the four salient features of the water entry cavity formed by decelerating spheres ($\Lambda > 0$). Relative to a sphere sinking at constant speed, the pinch-off depth, pinch-off time, and sphere depth at pinch-off decrease. Moreover, the pinch-off depth approaches the sphere depth at pinch-off, while the volume of the entrained bubble necessarily decreases. A theoretical prediction for the bubble volume may be made using Eqs. (11), (13), and (18)–(20). At the time of pinch-off, the cavity profile is given by Eq. (13) for $t = t_{\text{pinch}} - t(z)$ and the bubble volume by

$$\frac{V'_{\text{bubble}}}{R_0^3} = \pi \int_{z_{\text{pinch}}}^{Z(t_{\text{pinch}})} R^2(z)dz - \frac{2}{3}\pi. \quad (22)$$

A first-order Taylor series expansion of Eq. (22) about $\Lambda = 0$ yields

$$\frac{V'_{\text{bubble}}}{\frac{4}{3}\pi R_0^3} = \frac{1}{4}\alpha\mathcal{F} + \frac{3\sqrt{2}}{4}\alpha^{1/4}\mathcal{F}^{1/2} - \frac{1}{2} - \Lambda\left(\frac{3\sqrt{2}}{4}\alpha^{1/4}\mathcal{F}^{1/2}\right.$$
$$\left. + \frac{11\sqrt{2}}{10}\alpha^{5/4}\mathcal{F}^{3/2} + \frac{1}{2}\alpha\mathcal{F} + 3\sqrt{\alpha}\mathcal{F}\right), \quad (23)$$

where we have nondimensionalized the bubble volume by the sphere volume. For the case where the sphere deceleration is negligible, Eq. (23) reduces to

$$\frac{V'_{\text{bubble}}}{\frac{4}{3}\pi R_0^3} = \frac{3\sqrt{2}}{4}\alpha^{1/4}\left(1 + \frac{\sqrt{2}\alpha^{3/4}}{6}\mathcal{F}^{1/2}\right)\mathcal{F}^{1/2} - \frac{1}{2}. \quad (24)$$

We note that a similar expression was derived by Bergmann et al.[8] for the volume of air entrained by a disk sinking at constant speed,

$$\frac{V'_{\text{bubble}}}{h^3} \propto (1 + 0.26\mathcal{F}^{1/2})\mathcal{F}^{1/2}, \quad (25)$$

where h is the disk radius.

IV. DISCUSSION

A quantity of considerable interest to the military is the average deceleration of a sphere that impacts a water surface. Our combined experimental and theoretical investigation of the water-entry of low-density spheres has shown how a simple model for the sphere dynamics provides a reasonable

estimate of this quantity in terms of the impact parameters. The sphere dynamics is coupled to the cavity dynamics through hydrodynamic forces that are encapsulated by the drag and added-mass coefficients, respectively, C_d and C_m. By taking these coefficients to be constants, we infer the average sphere deceleration and obtain good agreement with experiment.

Our experimental study has revealed how the evolution of the water-entry cavity formed by an impacting sphere is altered by its deceleration. A theoretical model for the evolution of the cavity shape, introduced by Duclaux *et al.*,[9] has been generalized in order to describe the cavities formed by decelerating spheres and yields simple expressions for the pinch-off time and depth. This is made possible because the cavity dynamics is entirely determined by the sphere trajectory. One can thus use Eqs. (18)–(21) to rationalize the water-entry cavity formed by spheres whose densities are comparable to that of water and whose decelerations cannot be neglected.

The lowest-order theoretically predicted corrections to the dimensionless pinch-off time, pinch-off depth, and sphere depth at pinch-off vary in magnitude by the ratios 1:2:5. Thus, one expects changes in the pinch-off time between two spheres with different densities [Fig. 5(b)] to be least discernible, while their depth at pinch-off [Fig. 5(c)] to be the most. This is consistent with the experimental observations of Truscott and Techet,[10] who reported changes in the depth at pinch-off but not in the time of pinch-off.

Discrepancies between our experimental observations and theoretical predictions can be rationalized in terms of the assumed velocity potential. First, the two-dimensional geometry of the cavity obliged us to approximate the radial extent of the fluid motion;[9] shortcomings of this approximation are discussed by Bergmann *et al.*[8] Second, by assuming that the flow is purely radial, we are implicitly considering the limit in which the cavity depth is much greater than its breadth: the applicability of our model thus depends on the slenderness of the cavity and is expected to fail for weak impacts of relatively light spheres. A theoretical description of such impacts is left for future work.

In conclusion, our study has demonstrated that the dynamics of the air cavity formed in the wake of a sphere falling through the water surface can be altered considerably by the density of the sphere. While our study has focused on the events prior to pinch-off, one expects that the volume of entrained air will determine whether a dense sphere ultimately returns to the surface or sinks. The theoretically predicted bubble volume, given by Eq. (23), could thus be of use for modeling the mixing and transport of particles in the aqueous environment.

[1]A. May, "Water entry and the cavity-running behavior of missiles," Final technical report, Report No. A924020, NAVSEA Hydryballistics Advisory Committee, Silver Spring, MD, 1975, http://www.stormingmedia.us/92/9240/A924020.html.
[2]S. Ashley, "Warp drive underwater," Sci. Am. **284**, 70 (2001).
[3]O. M. Faltinsen, *Sea Loads on Ships and Offshore Structures* (Cambridge University Press, Cambridge, 1990), pp. 1–340.
[4]L. Rosellini, F. Hersen, C. Clanet, and L. Bocquet, "Skipping stones," J. Fluid Mech. **543**, 137 (2005).
[5]J. W. M. Bush and D. L. Hu, "Walking on water: Biolocomotion at the interface," Annu. Rev. Fluid Mech. **38**, 339 (2006).
[6]C. M. Seddon and M. Moatamedi, "Review of water entry with applications to aerospace structures," Int. J. Impact Eng. **32**, 1045 (2006).
[7]J. M. Aristoff and J. W. M. Bush, "Water entry of small hydrophobic spheres," J. Fluid Mech. **619**, 45 (2009).
[8]R. Bergmann, D. van der Meer, S. Gekle, A. van der Bos, and D. Lohse, "Controlled impact of a disk on a water surface: Cavity dynamics," J. Fluid Mech. **633**, 381 (2009).
[9]V. Duclaux, F. Caillé, C. Duez, C. Ybert, L. Bocquet, and C. Clanet, "Dynamics of transient cavities," J. Fluid Mech. **591**, 1 (2007).
[10]T. T. Truscott and A. H. Techet, "Water entry of spinning spheres," J. Fluid Mech. **625**, 135 (2009).
[11]A. May and J. C. Woodhull, "Drag coefficients of steel spheres entering water vertically," J. Appl. Phys. **19**, 1109 (1948).
[12]M. Lee, R. G. Longoria, and D. E. Wilson, "Cavity dynamics in high-speed water entry," Phys. Fluids **9**, 540 (1997).
[13]D. Gilbarg and R. A. Anderson, "Influence of atmospheric pressure on the phenomena accompanying the entry of spheres into water," J. Appl. Phys. **19**, 127 (1948).
[14]S. Gaudet, "Numerical simulation of circular disks entering the free surface of a fluid," Phys. Fluids **10**, 2489 (1998).
[15]J. W. Glasheen and T. A. McMahon, "Vertical water entry of disks at low Froude numbers," Phys. Fluids **8**, 2078 (1996).
[16]P. C. Hiemenz and R. Rajagopalan, *Principles of Colloid and Surface Chemistry* (Dekker, New York, 1997), pp. 1–650.
[17]C. Duez, C. Ybert, C. Clanet, and L. Bocquet, "Making a splash with water repellency," Nat. Phys. **3**, 180 (2007).
[18]S. Gekle, J. M. Gordillo, D. van der Meer, and D. Lohse, "High-speed jet formation after solid object impact," Phys. Rev. Lett. **102**, 034502 (2009).
[19]T. Grumstrup, J. B. Keller, and A. Belmonte, "Cavity ripples observed during the impact of solid objects into liquids," Phys. Rev. Lett. **99**, 114502 (2007).
[20]T. Miloh, "On the initial-stage slamming of a rigid sphere in a vertical water entry," Appl. Ocean Res. **13**, 43 (1991).
[21]G. K. Batchelor, *An Introduction to Fluid Dynamics* (Cambridge University Press, Cambridge, 2000), pp. 1–635.